

pubs.acs.org/JPCL Letter

# Thermodynamic Control over Molecular Aggregate Assembly Enables Tunable Excitonic Properties across the Visible and Near-Infrared

Arundhati P. Deshmukh, Austin D. Bailey, Leandra S. Forte, Xingyu Shen, Niklas Geue, Ellen M. Sletten, and Justin R. Caram\*



Cite This: J. Phys. Chem. Lett. 2020, 11, 8026-8033



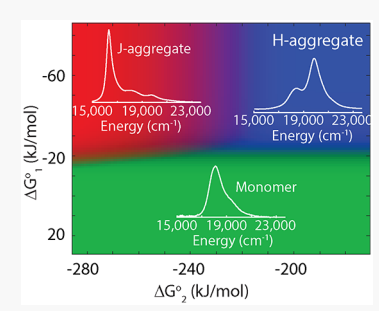
**ACCESS** 

III Metrics & More

Article Recommendations

s Supporting Information

ABSTRACT: Specific molecular arrangements within H-/J-aggregates of cyanine dyes enable extraordinary photophysical properties, including long-range exciton delocalization, extreme blue/red shifts, and excitonic superradiance. Despite extensive literature on cyanine aggregates, design principles that drive the self-assembly to a preferred H- or J-aggregated state are unknown. We tune the thermodynamics of self-assembly via independent control of the solvent/nonsolvent ratio, ionic strength, or dye concentration, obtaining a broad range of conditions that predictably stabilize the monomer (H-/J-aggregate). Diffusion-ordered spectroscopy, cryo-electron microscopy, and atomic force microscopy together reveal a dynamic equilibrium between monomers, H-aggregated dimers, and extended J-aggregated 2D monolayers. We construct a model that predicts the equilibrium composition for a range of standard Gibbs free energies, providing a vast aggregation space which we access using the



aforementioned solvation factors. We demonstrate the universality of this approach among several sheet-forming cyanine dyes with tunable absorptions spanning visible, near, and shortwave infrared wavelengths.

E xcitonic molecular aggregates are noncovalently assembled arrays of chromophores wherein monomeric transition dipole moments (TDMs) couple to form extended Frenkel excitons upon excitation. These aggregates exhibit emergent photophysical properties, such as extreme changes in their absorption, emission, and lifetimes which are tunable through the aggregate topology, molecular arrangement, and energy disorder. Large excitonic shifts afforded by long-range TDM coupling make the aggregates extremely tunable across the broad spectral range from the visible (400–700 nm) through the near and shortwave infrared ranges (NIR = 700–1000 nm and SWIR = 1000–2000 nm). Therefore, cyanine aggregates have extensive applications ranging from model systems for photosynthetic energy transfer, NIR/SWIR imaging, nonlinear optics, and plexitonics.

Understanding how these structures are stabilized and thereby control aggregate formation is a prerequisite to realizing potential technological and therapeutic applications. While many studies have elucidated the excitonic features of 2D and tubular cyanine aggregates and related it to their supramolecular structure, <sup>31–33</sup> little work has been done in understanding how these structures are stabilized. In Table 1, we summarize the diverse array of literature protocols used to prepare J-aggregates with the characteristic narrow red-shifted absorption for various benzothiazole cyanine dyes (Chart 1). While each procedure carries its advantages or disadvantages, it provides little rationale to approach the self-assembly of new chromophore aggregates. Here, we show that a general and straightforward approach

Table 1. Common Aggregation Strategies for Benzothiazole Cyanine Dyes and Examples of Dyes from the Literature Aggregated Using the Corresponding Strategy<sup>a</sup>

aggregate preparation strategy	examples of common aggregated benzothiazole dyes
direct dissolution (in water, salt solution, etc.)	Cy1, <sup>10</sup> Cy3, <sup>11,12</sup> THIATS, <sup>13</sup> Cy5, <sup>14</sup> Cy7 <sup>15</sup>
Langmuir-Blodgett films	Cy1 <sup>16,17</sup>
adsorption on a surface	Cy1, <sup>18</sup> Cy3, <sup>19,20</sup> THIATS <sup>21</sup>
thin films	THIATS, <sup>22,23</sup> Cy3, <sup>24,25</sup> Cy7 <sup>26</sup>
crystallization on the interface	Cy3 <sup>27</sup>
DNA or polymer templating	Cy1, <sup>28</sup> Cy3, <sup>29</sup> Cy5, <sup>29,30</sup> Cy7 <sup>29</sup>
independent control of solvation	Cy7 <sup>5</sup> (previous work)
conditions	Cy3, Cy5, Cy7 (this work)

"General structures of the dyes are shown in Chart 1. To simplify the diversity in structures, we group the dyes according to the length of the cyanine bridge.

based on the independent control of solvation conditions allows us to directly tune the thermodynamics of self-assembly of

Received: July 19, 2020 Accepted: September 2, 2020 Published: September 2, 2020





Chart 1. General Structure of Benzothiazole Cyanine Dyes Aggregated Using the Strategies Listed in Table 1, with Some Examples of the Substituents

cyanine aggregates in solution. A simple thermodynamic model allows us to construct a phase diagram for the aggregation of cyanine dyes. Thermodynamic control of self-assembly allows us to selectively stabilize an aggregate morphology under flexible conditions (such as extremely high or low dye concentrations), unlike previous methods which work under specific conditions. This makes the aggregates amenable toward a broader scope of experimental techniques, such as diffusion-ordered spectroscopy (DOSY), and applications in devices.

Aggregation Studies. We focus on benzothiazole cyanine dyes that show a simple three-component equilibrium among monomers, H-aggregates, and J-aggregates which can be easily distinguished using their characteristic absorptions (Figure 1a). We use Cy3-Et (Figure 1b) as a model system that is structurally

close to the commonly studied THIATS.<sup>22</sup> Several strategies have been used to aggregate THIATS and similar dyes, summarized in Table 1, including direct dissolution in water, <sup>15</sup> adsorption on silver halides, <sup>19</sup> and spin coating.<sup>22</sup> Here, we stabilize Cy3-Et aggregates under a variety of conditions by independently controlling different solvation conditions. While salt addition and solvent/nonsolvent mixtures are extensively utilized to drive aggregation, our systematic implementation presents a tunable range of conditions to stabilize a particular structure. We make a monomer solution in methanol and disperse it into water (with or without NaCl), a more generalized modification of the well-known "alcoholic route." We use these parameters to access the aggregation phase space and plot the resulting absorption spectra in Figure 1c.

We vary the (i) final dye concentration (top panel); (ii) solvent/nonsolvent ratio (middle panel); and (iii) ionic strength by adding salt (bottom panel) while keeping the other two factors constant. Unsurprisingly, we find that higher dye concentrations favor H-aggregation followed by J-aggregation. In addition, high % MeOH ( $\sim$ 70%) and low dye concentrations always favor monomeric state. As we decrease the % MeOH or increase the salt concentration, we observe a gradual transformation of monomers to H-aggregates and finally to J-aggregates. Our results are consistent with the hypothesis that ionic-strength-induced dielectric screening and hydrophobic interactions (lower % MeOH) stabilize extended aggregates.  $^{35}$ 

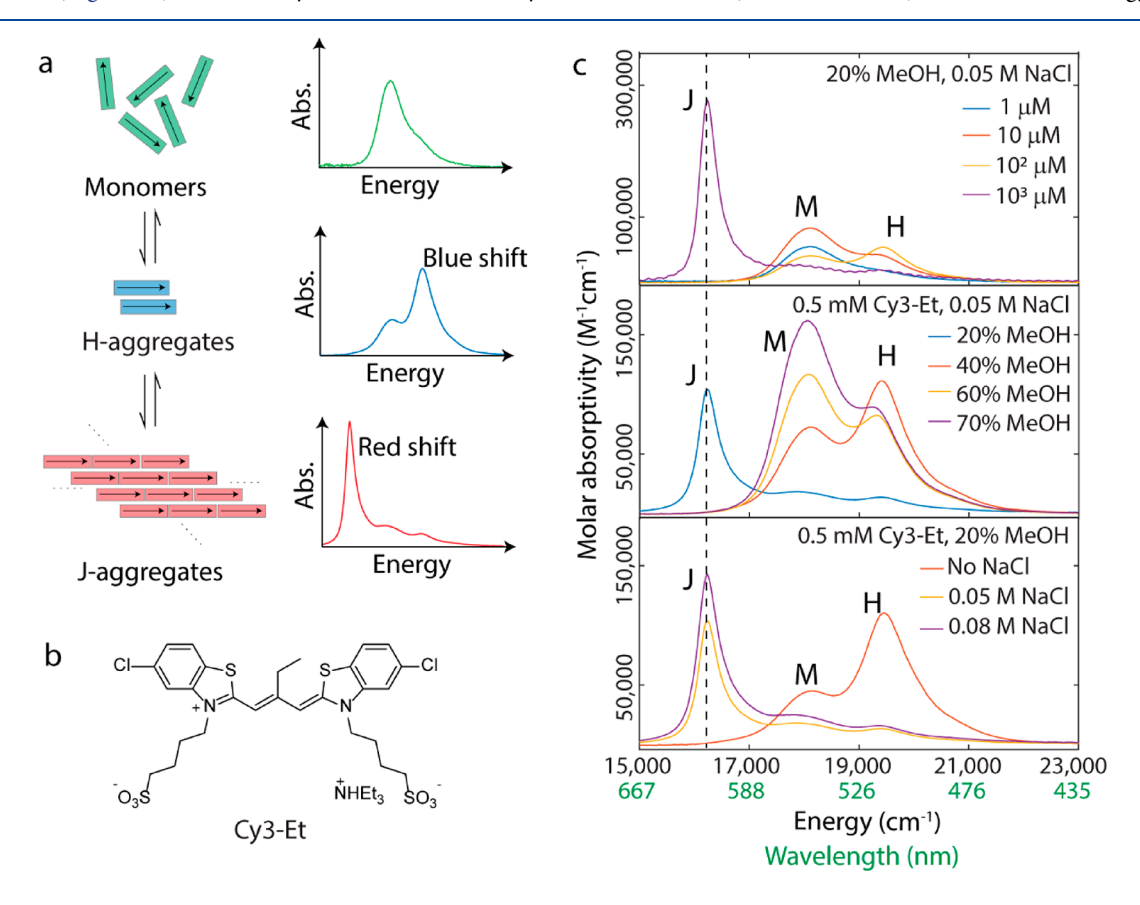


Figure 1. (a) Schematic showing the transformation of monomers to H-aggregates (dimers) to J-aggregates (extended monolayer sheets) and characteristic line shapes of absorption spectra of the corresponding species in solution. (b) Structure of dye Cy3-Et. (c) Absorption spectra taken  $\sim$ 24 h after sample preparation, where a predissolved monomer solution in methanol was injected into aqueous solution with or without NaCl while varying the (top) dye concentration, (middle) v/v methanol/water ratio, and (bottom) salt concentration. In each case, the other two factors were kept constant.

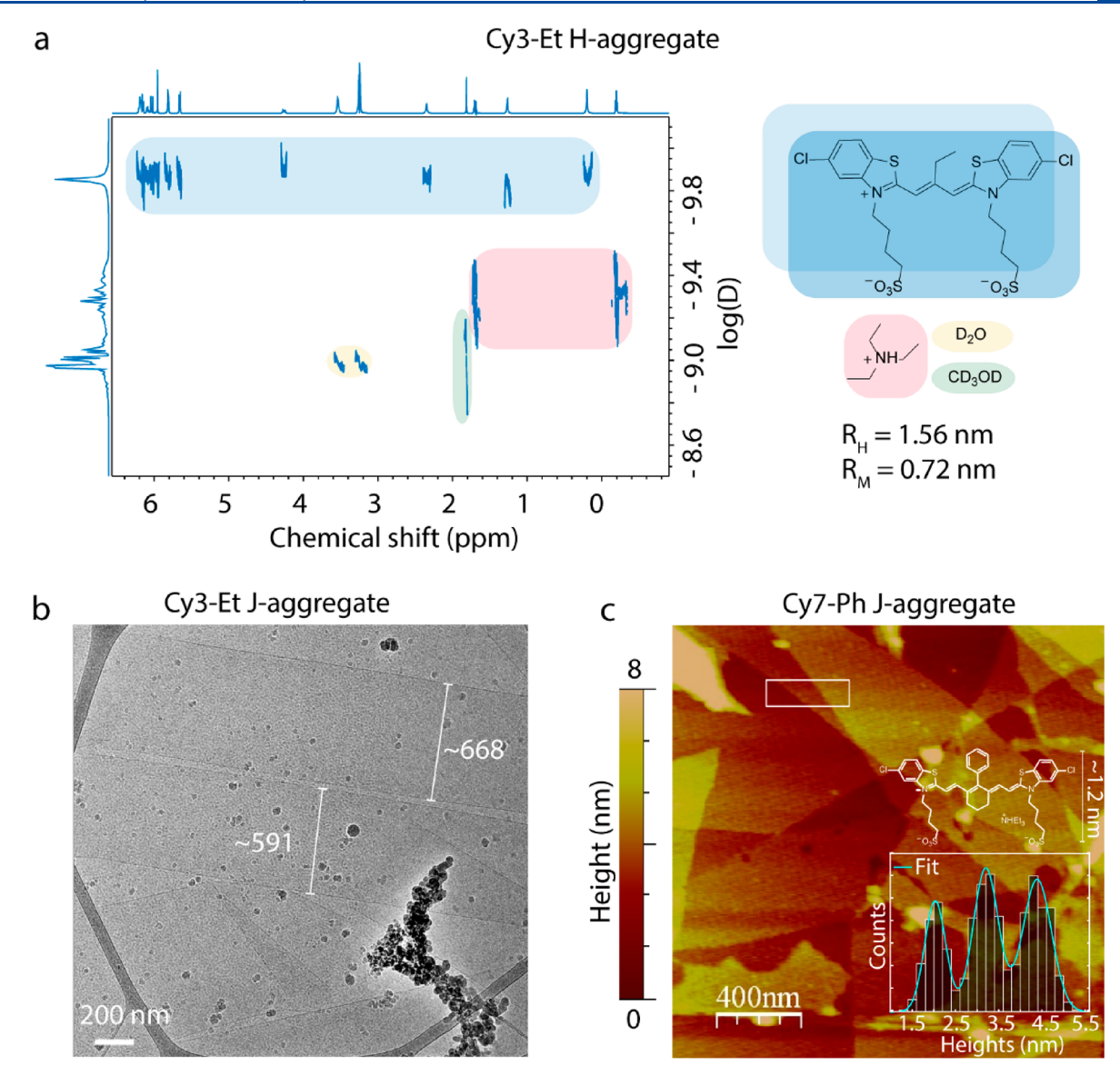


Figure 2. (a)  $^{1}$ H diffusion-ordered spectroscopy (DOSY) of Cy3-Et H-aggregates at a 1 mM concentration prepared in 90% D<sub>2</sub>O and 10% MeOD. Comparing the hydrodynamic radius with a monomer suggests dimer morphology. (b) Cryoelectron microscopy image of a vitrified Cy3-Et J-aggregate depicting sheet-like morphology. The numbers indicate sheet widths in nanometers. (c) Atomic force microscopy image of Cy7-Ph J-aggregates with a histogram of the heights (bottom inset) enclosed in the white rectangle. The histogram is fit to a sum of three Gaussians (cyan line) with  $R^2 = 0.9695$ . The height of a single layer obtained from the histogram matches the height of a single molecule (top inset) indicating monolayer sheets.

Moreover, this far simpler and easily generalizable approach yields similar narrow red-shifted absorption line shapes for Jaggregates, as seen in previous methods (Table 1), indicating that we are able to access the similar J-aggregate microstructures that lead to this characteristic line shape with a higher degree of control.

Characterization of H- and J-Aggregate Structures. The use of different solvation conditions to stabilize a desired H- or J-state allows us to develop preparations that are amenable to characterization tools requiring high concentrations of a single species. For example, smaller aggregate species such as dimers and oligomers are too small for characterization tools such as cryo-electron microscopy (cryoEM) and atomic force microscopy (AFM). Multidimensional NMR methods such as diffusion-ordered spectroscopy (DOSY) typically require very high concentrations where fully aggregated species tend to be more dominant than smaller aggregates. Using the methods

outlined above, we were able to perform DOSY on Haggregates, stabilizing the H-aggregate at a concentration of 1 mM by retaining a low volume fraction of deuterated methanol (10:90 MeOD/D2O, no NaCl). In Figure 2a, all of the peaks corresponding to the aggregate emerge at a single diffusion constant of  $1.32 \times 10^{-10}$  m<sup>2</sup>/s while faster diffusing species such as counterions and solvent show up at higher diffusion constants. A comparison with the DOSY spectrum of the monomer, in Supporting Information (SI) Figure S1, shows that the Haggregate is about twice the size of the monomer (SI Table S1). We thus conclude that the H-aggregate is a dimer consistent with previous concentration-dependent absorption studies. 11 For the red-shifted J-aggregates, we perform cryoEM and AFM. CryoEM demonstrates extended rectilinear sheets with average dimensions of 500-1000 nm by several micrometers. AFM height analysis (Figure 2c) confirms monolayer structures with molecular plane perpendicular to the plane of the sheet (SI

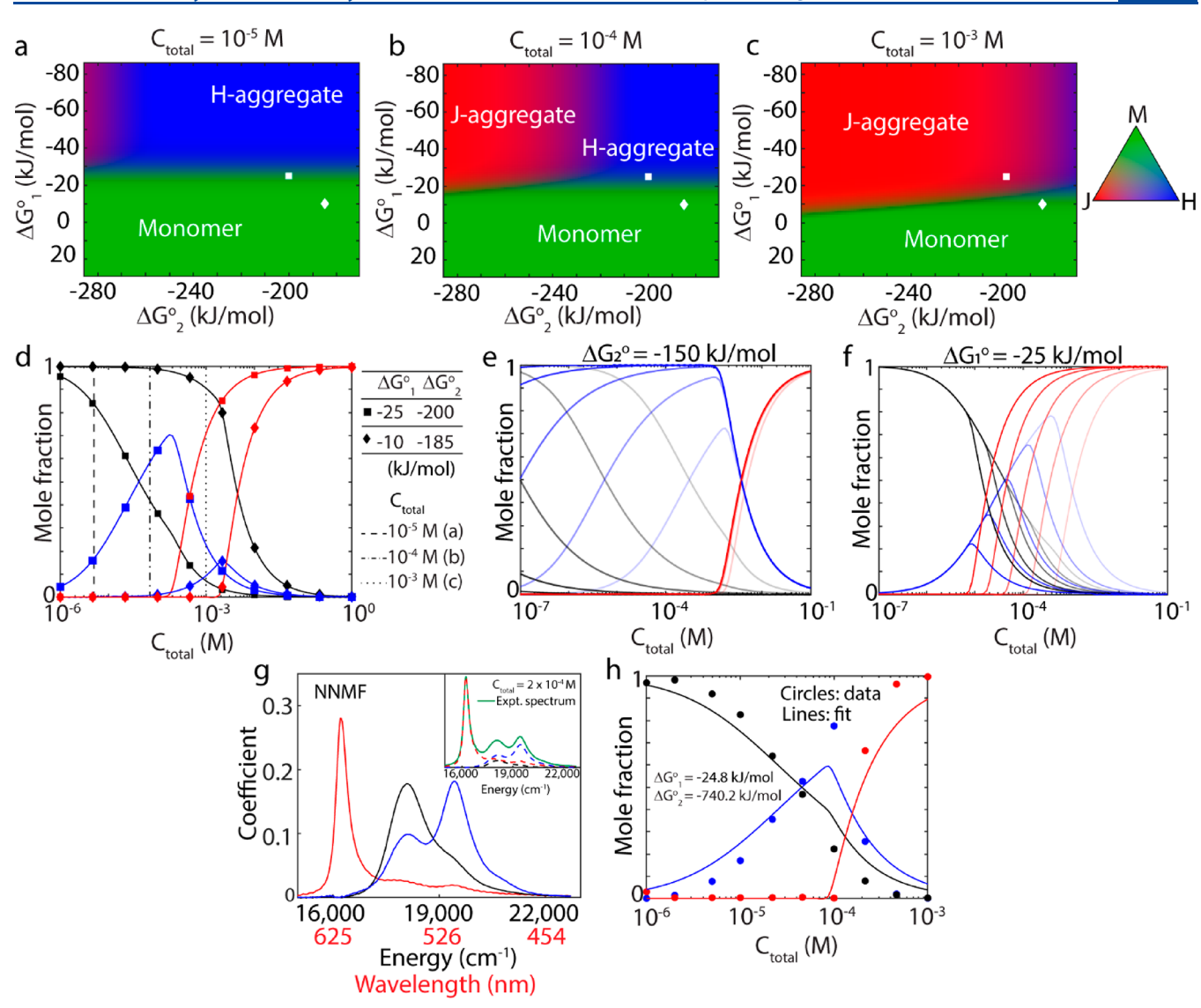


Figure 3. Prediction of equilibrium composition using the three-component model. (a-c) Maps showing the variation of equilibrium composition as a function of standard Gibbs free energies of monomer to H-aggregate equilibrium  $(\Delta G_1^\circ)$  and H-aggregate to J-aggregate  $(\Delta G_2^\circ)$  for different total dye concentrations  $(C_{\text{total}})$ ,  $n_1=2$ , and  $n_2=10$ . (a)  $C_{\text{total}}=10^{-5}$  M, (b)  $C_{\text{total}}=10^{-4}$  M, and (c)  $C_{\text{total}}=10^{-3}$  M. The color of each pixel denotes the composition shown in the ternary plot on the right with the RGB value corresponding to mole fractions of the J-aggregate, monomer, and H-aggregate. (d–f) Evolution of mole fractions of monomer (black), H-aggregate (blue), and J-aggregate (red) with  $C_{\text{total}}$ . (d) For two points on  $\Delta G^\circ$  maps denoted by squares  $(\Delta G_1^\circ = -25, \Delta G_2^\circ = -200 \text{ kJ/mol})$  and diamonds  $(\Delta G_1^\circ = -10, \Delta G_2^\circ = -185 \text{ kJ/mol})$ , vertical lines correspond to the  $C_{\text{total}}$  values in a–c. (e)  $\Delta G_1^\circ$  varies from -60 kJ/mol (darkest) to -20 kJ/mol (lightest) and  $\Delta G_2^\circ = -180 \text{ kJ/mol}$ . (f)  $\Delta G_2^\circ$  varies from -300 kJ/mol (darkest) to -180 kJ/mol mol (lightest) and  $\Delta G_1^\circ = -25 \text{ kJ/mol}$ . (g) Basis vectors obtained from non-negative matrix factorization (NNMF) of the experimental concentration dependence data (SI Figure SS). (Inset) Example of an experimental spectrum (green) with the decomposition into three NNMF vectors (dashed lines) corresponding to the monomer (black), H-aggregate (blue), and J-aggregate (red). (h) Experimental mole fractions obtained from NNMF (circles) and the fitted mole fraction curves from the three-component model (lines).

section 1.2). We do not observe any conversion to nanotubes or other morphologies over a week for Cy7-Ph J-aggregates (SI Figure S3). H-aggregates occasionally show a slow conversion to J-aggregates over long times, which may be due to solvent evaporation. As this conversion is very slow, we treat the H-aggregate as being in quasi-equilibrium with the monomer and J-aggregate.

Three-Component Equilibrium Model. We construct a thermodynamic model that describes the energetic landscape governing the self-assembly of dimerized H-aggregates and sheet-like J-aggregates. On the basis of the observations in Figure 1c, we consider two general equilibria as follows.

$$n_1 \mathbf{M} \rightleftharpoons \mathbf{H}$$
 (1)

$$n_2 H \rightleftharpoons J$$
 (2)

M, H, and J denote the monomer, H-aggregate, and J-aggregate species, respectively.  $n_1$  denotes the number of monomers in an H-aggregate, and  $n_1n_2$  is the total number of monomers in the J-aggregate. We use subscripts 1 and 2 for the equilibrium constants ( $K_{\rm eq}$ ) and standard Gibbs free energies ( $\Delta G^{\circ}$ ) of equilibria 1 and 2, respectively. The respective equilibrium constants can be written as

$$K_1 = \frac{C_H}{C_M^{n_1}} \tag{3}$$

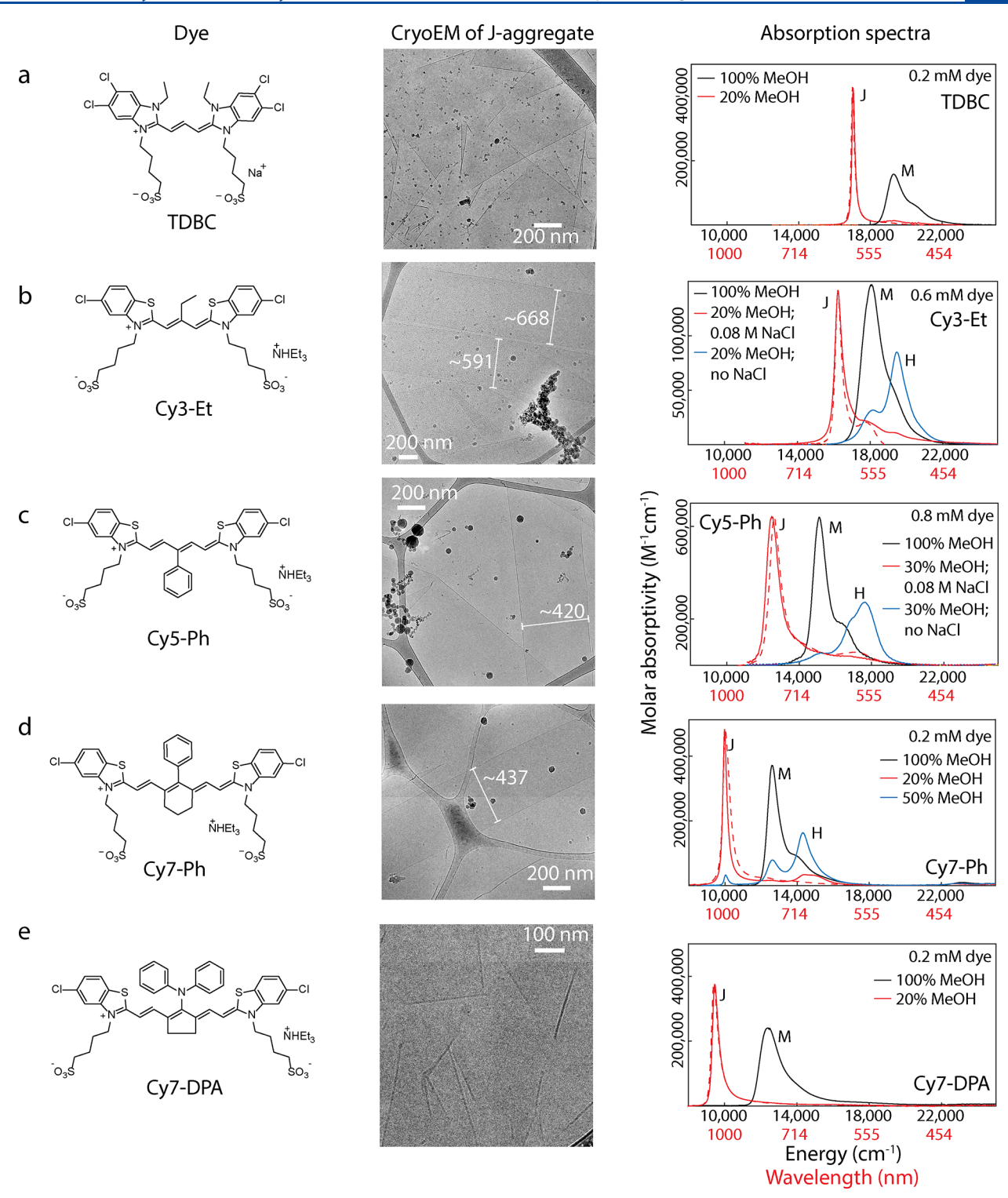


Figure 4. Applying the principles from this work to several dyes with absorption tunability from the visible through SWIR: (left) dye structures; (center) cryoelectron microscopy image of the 2D sheet aggregates; and (right) absorption spectra of the monomer (black), H-aggregates (blue), redshifted 2D aggregates (red, solid line), and sugar-matrix-stabilized 2D aggregates (red dashed line). The numbers on cryoEM images indicate sheet widths in nanometers. Absorption spectra of sugar matrix samples are arbitrarily scaled to compare the line shapes with solution spectra.

$$K_2 = \frac{C_{\rm J}}{C_{\rm H}^{n_2}} \tag{4}$$

The total concentration,  $C_{\text{tot}}$  is defined as

$$C_{\text{tot}} = C_{\text{M}} + n_1 C_{\text{H}} + n_1 n_2 C_{\text{I}}$$

where 
$$C_{\rm M}$$
,  $C_{\rm H}$ , and  $C_{\rm J}$  denote the concentrations of monomer, H-aggregate, and J-aggregate, respectively. Upon substitution and rearrangement (complete derivation in SI Section 2), we arrive at the characteristic polynomial of  $C_{\rm M}$  with respect to total concentration, equilibrium constants, and aggregate size.

$$n_1 n_2 K_2 K_1^{n_2} C_M^{n_1 n_2} + n_1 K_1 C_M^{n_1} + C_M - C_{\text{tot}} = 0$$
 (6)

(5)

This high-order polynomial will always have exactly one real positive root (proof in SI Section 2), which allows us to use standard root-finding methods to find  $C_{\rm M}$  for a given set of parameters. Mole fractions of each species  $(\chi_{\rm M},\chi_{\rm H},{\rm and}\,\chi_{\rm J})$  can be calculated for any combination of  $\Delta G^{\circ}$  using eqs 3–5). Thus, we can uniquely define the equilibrium composition of the solution for any combination of standard Gibbs free energies. This characteristic polynomial is independent of the choice of pathway to aggregation, whether through it goes from monomer directly to J-aggregate or the dimer forms combine to form the J-aggregate sheet (details in SI Section 2.3).

In Figure 3a—c, we map the ternary equilibrium composition as we change the standard Gibbs free energies of H-dimerization on the x axis and extended 2D J-aggregate formation on the yaxis. We note that these Gibbs free energies are not truly independent in our experiment; the solvation and ionic strength may affect both, to differing degrees. We set  $n_1 = 2$  based on our DOSY results (Figure 2a) and  $n_2 = 10$ , representing a total aggregation number of 20 in extended J-aggregates. While this number greatly underestimates the number of J-aggregated monomers, it captures the sharp onset of J-aggregation as a function of concentration and is amenable to root-finding algorithms. Each point on these maps represents a different equilibrium condition for a fixed concentration. Given a set of experimental  $\Delta G^{\circ}$  values for any system, our model predicts the equilibrium composition at any concentration (Figure 3a-c). Changing solvation conditions such as % MeOH or salt concentration directly affects  $\Delta G_1^{\circ}$  and  $\Delta G_2^{\circ}$  and spans this phase space, as might adding substituents to the chromophore. The direct transition from H-aggregate to J-aggregate involves a change in  $\Delta G_2^{\circ}$  (corresponding to extended aggregate formation). This suggests that increasing the ionic strength at low % MeOH (Figure 1c) mostly changes  $\Delta G_2^{\circ}$ . At highly negative  $\Delta G_2^{\circ}$ , we observe a direct transition from monomer to Jaggregate upon reducing  $\Delta G_1^{\circ}$ .

We pick two fixed points on the maps in Figure 3a-c corresponding to  $\Delta G_1^{\circ} = -25$ ,  $\Delta G_2^{\circ} = -200$  kJ/mol (square), and  $\Delta G_1^{\circ} = -10$ ,  $\Delta G_2^{\circ} = -185$  kJ/mol (diamond) and plot them with the other total chromophore concentrations in Figure 3d. In all cases, the J-aggregates require a certain threshold concentration where we observe a sharp increase or "turn-on" in the J-aggregate mole fraction. This nonsigmoidal nature of Jaggregate mole fraction curves is the direct result of the formation of large aggregates.<sup>35</sup> SI Figure S4 shows mole fractions as a function of  $n_2$ , which depicts the delayed and sharper turn-on in J-aggregation as a function of aggregate size. As increasing ionic strength transitions from the H- to the Jaggregate, we hypothesize that it primarily affects  $\Delta G_2^{\circ}$  due to additional charge screening. Figure 3e,f demonstrates that  $\Delta G_1^{\circ}$ does not affect the J-aggregate onset but  $\Delta G_2^{\circ}$  changes are coincident with a sharp decrease in the monomer and Haggregate.

This sharp turn-on in the J-aggregate is a clear indication of cooperative self-assembly akin to a phase transition or reaching a critical micelle concentration. We attribute the cooperativity to the 2D nature of sheet-like aggregates: the number of potential molecular contacts increases linearly with the aggregate size. Unlike traditional 1D aggregates, cooperative assembly in 2D can be achieved without invoking a change in chemical potential for every additional monomer. Due to additional contacts in 2D aggregates, we require more charge screening as evident from our experiment (Figure 1c) where 2D aggregates are stabilized by adding salt. Our results suggest that

many systems can be aggregated into 2D brick-layer sheets simply by stabilizing  $\Delta G_2^{\circ}$  relative to  $\Delta G_1^{\circ}$ , for example, through control of the solvent to nonsolvent ratio or by adding salt

In order to show quantitative agreement between our model and experiment, we determine the concentration dependence of Cy3-Et at 20% MeOH and 0.05 M NaCl (SI Figure S5). Since there are three overlapping spectra, we decompose our observed spectra into J, H, and M spectra via non-negative matrix factorization (NNMF, SI Section 4).<sup>38</sup> We obtain three basis vectors (Figure 3g, example decomposition shown in inset), which are consistent with experimental spectra of the monomer and published spectra for dimer H-aggregates and Jaggregates. 11 We plot the mole fractions obtained from NNMF for this concentration series in Figure 3h (circles), capturing the sharp increase in the J-aggregate at 10<sup>-4</sup> M. Finally, we fit the mole fraction data for all three components simultaneously to arrive at Gibbs free energies of  $\Delta G_1^{\circ}$  = -24.8 and  $\Delta G_2^{\circ} = -740.2$  kJ/mol (SI Section 5). This  $\Delta G_1^{\circ}$  value is very close to the previously reported dimerization energy for THIATS ( $\Delta G_1^{\circ} = -25.9 \text{ kJ/mol}$ ). The highly negative  $\Delta G_2^{\circ}$ , indicating the strong favorability of extended 2D aggregate formation, is ascribed to the increased number of interactions in 2D aggregates.<sup>37</sup>

Generality of Self-Assembly Principles. We demonstrate that the principles for self-assembly used here are truly generalizable and are also extendable to other families of cyanine dyes such as benzimidazole cyanines. Figure 4 shows a list of cyanine dyes that form 2D sheet-like aggregates with tunable absorption from the visible through SWIR. In all of these cases, the aggregation behavior followed similar trends where lower % MeOH (20-30%) gave extended J-aggregated sheets, and the optimal salt and dye concentrations differ slightly among individual dyes. With the exceptions of TDBC and Cy7-DPA, we also observe a similar H-aggregate peak at 50% MeOH. Particularly, larger dye molecules such as Cy7-DPA and Cy7-Ph aggregate readily without any need for salt, whereas Cy3-Et and Cy5-Ph need slightly higher dye concentrations with added salt, suggesting that higher surface areas lead to stronger van der Waals interactions. A particular example of the well-known benzimidazole cyanine dye, TDBC is shown in Figure 4a. TDBC is also known to form sheet aggregates that have garnered interest in excitonic energy transfer and plexitonics. We show that the principles outlined above can also be used to tune the selfassembly of TDBC into sheet-like J-aggregates (Figure S6). TDBC and Cy7-DPA do not go through an H-aggregate state likely due to the ethyl groups (in the case of TDBC) and the bulky diphenylamine group (in the case of Cy7-DPA) that might sterically hinder cofacial stacking. Furthermore, we show that all of the 2D aggregates in Figure 4 can be stabilized in a sugar matrix (dashed lines), which is known to protect the aggregates against photo and air damage,<sup>39</sup> preserving the characteristic excitonic features while facilitating cryogenic and high excitation flux spectroscopies on the aggregates.

We conclude that the aggregation strategy based on independently controlling the solvent to nonsolvent ratio and the salt or dye concentration provides a general and tunable avenue for selectively stabilizing an aggregate morphology for the broad class of cyanine dyes. Our approach avails a broad range of aggregation conditions to stabilize a desired morphology, which in turn controls the excitonic properties. In addition, the tunability over a vast aggregation space enables new structural characterization techniques such as DOSY and broadens the application space. For example, aggregating at

lower concentrations through a lower nonsolvent ratio can be used to control the optical density of aggregate antennas in thin films.

We explain the conserved aggregation trends on the basis of a simple three-component equilibrium model and gain insight into the thermodynamics of the self-assembly process. Our results show that the ionic strength mainly affects  $\Delta G_2^\circ$ , enabling a direct transition from dimer H-aggregates to extended J-aggregates at the same dye concentration and solvent composition, likely by stabilizing larger charged structures. The solvent to nonsolvent ratio, on the other hand, likely affects both  $\Delta G_1^\circ$  and  $\Delta G_2^\circ$  because it can induce both H- and J-aggregation depending on the available dye concentration. NNMF untangles the constituent spectra and shows that we can achieve excellent agreement between model and experiment. Finally, we show that solvation control can be extended to several sheet-forming cyanine dyes, thus enabling a tunable library with absorptions ranging from the visible to SWIR.

The kinetics and thermodynamics of the aggregation of chromophores are topics of extensive research, mostly focused on the 1D  $\pi$ -stacking structures of porphyrins and perylene bisimides. 35,40,41 However, extended 2D aggregates have unique features not reproduced in linear aggregates. The number of pairwise interactions between an aggregate and a monomer is proportional to the aggregate size in the 2D case, whereas it is a constant for linear aggregates. By analogy to bilayer formation in surfactants, one observes a near phase transition above a set concentration of dye in 2D aggregates.<sup>37</sup> In linear aggregates with pairwise interactions, phase transitions are rigorously forbidden.<sup>37</sup> Despite the rich excitonic properties and diverse applications of cyanine dye aggregates, application of the thermodynamic self-assembly principles to the broad class of cyanine dye aggregates is unprecedented. Overall, 2D aggregation provides a unique platform for even more stable structures at lower concentrations while retaining the excitonic features of J-aggregates, and the broad class of cyanine dyes is an excellent avenue for this. The simple and broadly applicable principles for aggregation presented here provide the first step toward realizing many potential applications of molecular aggregates.

### ASSOCIATED CONTENT

### Supporting Information

The Supporting Information is available free of charge at https://pubs.acs.org/doi/10.1021/acs.jpclett.0c02204.

Characterization of aggregates (DOSY, AFM, absorption spectra over a long time), three-component equilibrium model derivation, effect of aggregation number, nonnegative matrix factorization, experimental Gibbs free energies, TDBC aggregation studies, and experimental section (PDF)

# AUTHOR INFORMATION

# **Corresponding Author**

Justin R. Caram — Department of Chemistry and Biochemistry, University of California, Los Angeles, Los Angeles, California 90095, United States; orcid.org/0000-0001-5126-3829; Email: jcaram@chem.ucla.edu

### **Authors**

- Arundhati P. Deshmukh Department of Chemistry and Biochemistry, University of California, Los Angeles, Los Angeles, California 90095, United States
- Austin D. Bailey Department of Chemistry and Biochemistry, University of California, Los Angeles, Los Angeles, California 90095, United States
- Leandra S. Forte Department of Chemistry and Biochemistry, University of California, Los Angeles, Los Angeles, California 90095, United States
- Xingyu Shen Department of Chemistry and Biochemistry, University of California, Los Angeles, Los Angeles, California 90095, United States; College of Chemistry and Molecular Engineering, Peking University, Beijing 100871, P. R. China
- Niklas Geue Department of Chemistry and Biochemistry, University of California, Los Angeles, Los Angeles, California 90095, United States; Department of Chemistry and Mineralogy, Leipzig University, 04103 Leipzig, Germany
- Ellen M. Sletten Department of Chemistry and Biochemistry, University of California, Los Angeles, Los Angeles, California 90095, United States; orcid.org/0000-0002-0049-7278

Complete contact information is available at: https://pubs.acs.org/10.1021/acs.jpclett.0c02204

#### Notes

The authors declare no competing financial interest.

### ACKNOWLEDGMENTS

This work was supported by NSF CHE grant no. 1905242 and a faculty research grant (UCLA Academic Senate). A.P.D. is grateful for a UCLA Chemistry and Biochemistry Excellence in Research Fellowship and an SG fellowship for financial support. The authors thank the Materials Characterization Laboratory, UCLA for instrumentation and Dr. Timothy L. Atallah, UCLA for constructive comments. A.P.D. thanks Sudhanshu Srivastava, UCSB for discussions on statistical methods. X.S. is grateful for a CSST (Cross-Disciplinary Scholars in Science and Technology) scholarship. The authors acknowledge the use of instruments at the Electron Imaging Center for NanoMachines supported by the NIH (1S10RR23057) and CNSI at UCLA.

## REFERENCES

- (1) Kasha, M. Energy Transfer Mechanisms and the Molecular Exciton Model for Molecular Aggregates. *Radiat. Res.* **1963**, *20* (1), 55–71.
- (2) Davydov, A. S. The Theory of Molecular Excitons. Sov. Phys. Uspekhi 1964, 7 (2), 145–178.
- (3) Fidder, H.; Knoester, J.; Wiersma, D. A. Optical Properties of Disordered Molecular Aggregates: A Numerical Study. *J. Chem. Phys.* **1991**, 95 (11), 7880–7890.
- (4) Bricks, J. L.; Slominskii, Y. L.; Panas, I. D.; Demchenko, A. P. Fluorescent J-Aggregates of Cyanine Dyes: Basic Research and Applications Review. *Methods Appl. Fluoresc.* **2018**, *6* (1), No. 012001.
- (5) Deshmukh, A. P.; Koppel, D.; Chuang, C.; Cadena, D. M.; Cao, J.; Caram, J. R. Design Principles for Two-Dimensional Molecular Aggregates Using Kasha's Model: Tunable Photophysics in Near and Short-Wave Infrared. *J. Phys. Chem. C* **2019**, *123* (30), 18702–18710.
- (6) Sun, C.; Li, B.; Zhao, M.; Wang, S.; Lei, Z.; Lu, L.; Zhang, H.; Feng, L.; Dou, C.; Yin, D.; et al. J-Aggregates of Cyanine Dye for NIR-II in Vivo Dynamic Vascular Imaging beyond 1500 Nm. *J. Am. Chem. Soc.* **2019**, *141* (49), 19221–19225.
- (7) Eisele, D. M.; Arias, D. H.; Fu, X.; Bloemsma, E. A.; Steiner, C. P.; Jensen, R. A.; Rebentrost, P.; Eisele, H.; Tokmakoff, A.; Lloyd, S.; et al.

- Robust Excitons Inhabit Soft Supramolecular Nanotubes. Proc. Natl. Acad. Sci. U. S. A. 2014, 111 (33), E3367–E3375.
- (8) Cacciola, A.; Triolo, C.; Di Stefano, O.; Genco, A.; Mazzeo, M.; Saija, R.; Patanè, S.; Savasta, S. Subdiffraction Light Concentration by J-Aggregate Nanostructures. *ACS Photonics* **2015**, *2*, 971–979.
- (9) Zhong, X.; Chervy, T.; Wang, S.; George, J.; Thomas, A.; Hutchison, J. A.; Devaux, E.; Genet, C.; Ebbesen, T. W. Non-Radiative Energy Transfer Mediated by Hybrid Light-Matter States. *Angew. Chem.*, Int. Ed. **2016**, 55 (21), 6202–6206.
- (10) Bücher, H.; Kuhn, H. Scheibe Aggregate Formation of Cyanine Dyes in Monolayers. *Chem. Phys. Lett.* **1970**, *6* (3), 183–185.
- (11) Takahashi, D.; Oda, H.; Izumi, T.; Hirohashi, R. Substituent Effects on Aggregation Phenomena in Aqueous Solution of Thiacarbocyanine Dyes. *Dyes Pigm.* **2005**, *66* (1), 1–6.
- (12) Chen, X.; Chen, Y. H.; Qin, J.; Zhao, D.; Ding, B.; Blaikie, R. J.; Qiu, M. Mode Modification of Plasmonic Gap Resonances Induced by Strong Coupling with Molecular Excitons. *Nano Lett.* **2017**, *17* (5), 3246–3251.
- (13) Scheblykin, I. G.; Varnavsky, O. P.; Verbouwe, W.; De Backer, S.; Van Der Auweraer, M.; Vitukhnovsky, A. G. Relaxation Dynamics of Excitons in J-Aggregates Revealing a Two-Component Davydov Splitting. *Chem. Phys. Lett.* **1998**, 282 (3–4), 250–256.
- (14) Berlepsch, H. V.; Böttcher, C. Tubular J-Aggregates of a New Thiacarbocyanine Cy5 Dye for the Far-Red Spectral Region-a Spectroscopic and Cryo-Transmission Electron Microscopy Study. *Phys. Chem. Chem. Phys.* **2018**, 20 (28), 18969–18977.
- (15) Berlepsch, H. V.; Böttcher, C. Cryo-Transmission Electron Microscopy Reveals Mesoscopic H- and J-Aggregates of near Infrared Cyanine Dyes. *J. Photochem. Photobiol.*, A **2010**, 214 (1), 16–21.
- (16) Yamaguchi, A.; Kotnetani, N.; Yonezawa, Y. Luminescence Properties of the Mixed J-Aggregate of Oxacyanine Dye and Thiacyanine Dye. Formation of a Persistence-Type Aggregate. *J. Phys. Chem. B* **2005**, *109* (4), 1408–1414.
- (17) Debnath, P.; Chakraborty, S.; Deb, S.; Nath, J.; Dey, B.; Bhattacharjee, D.; Soda, H.; Tominaga, M.; Suzuki, Y.; Kawamata, J.; et al. Effect of Nano Clay Laponite on Stability of SHG Active J-Aggregate of a Thiacyanine Dye onto LB Films. *Appl. Clay Sci.* **2017**, 147, 105–116.
- (18) Laban, B.; Vodnik, V.; Dramićanin, M.; Novaković, M.; Bibić, N.; Sovilj, S. P.; Vasić, V. M. Mechanism and Kinetics of J-Aggregation of Thiacyanine Dye in the Presence of Silver Nanoparticles. *J. Phys. Chem. C* **2014**, *118* (40), 23393–23401.
- (19) Kemnitz, K.; Yoshihara, K.; Suzumoto, T.; Tani, T.; Lindrum, M.; Moll, J.; Daehne, S. Primary Photophysical Processes InJ-Aggregates of Spectral Sensitisers. *Proc. Indian Acad. Sci., Chem. Sci.* **1993**, *105* (6), 783–795.
- (20) Zhang, F.; Sautter, K.; Larsen, A. M.; Findley, D. A.; Davis, R. C.; Samha, H.; Linford, M. R. Chemical Vapor Deposition of Three Aminosilanes on Silicon Dioxide: Surface Characterization, Stability, Effects of Silane Concentration, and Cyanine Dye Adsorption. *Langmuir* **2010**, *26* (18), 14648–14654.
- (21) Oh, J. W.; Kumazaki, S.; Rubtsov, I. V.; Suzumoto, T.; Tani, T.; Yoshihara, K. Ultrafast Energy Transfer in J-Aggregate on AgBr Microcrystals: Its Dependence on Dye Coverage. *Chem. Phys. Lett.* **2002**, 352 (5–6), 357–362.
- (22) Hasegawa, D.; Nakata, K.; Tokunaga, E.; Okamura, K.; Du, J.; Kobayashi, T. Vibrational Energy Flow between Modes by Dynamic Mode Coupling in THIATS J-Aggregates. *J. Phys. Chem. A* **2013**, *117* (45), 11441–11448.
- (23) Tanaka, Y.; Yoshikawa, H.; Masuhara, H. Thiacarbocyanine Dye J-Aggregation in Optical Trapping Potential. In *Optical Trapping and Optical Micromanipulation III*; Dholakia, K., Spalding, G. C., Eds.; SPIE, 2006; Vol. 6326, p 63262J.
- (24) Chevrier, K.; Benoit, J. M.; Symonds, C.; Paparone, J.; Laverdant, J.; Bellessa, J. Organic Exciton in Strong Coupling with Long-Range Surface Plasmons and Waveguided Modes. *ACS Photonics* **2018**, *5* (1), 80–84.
- (25) Prokhorov, V. V.; Pozin, S. I.; Lypenko, D. A.; Perelygina, O. M.; Mal'tsev, E. I.; Vannikov, A. V. Molecular Arrangements in Two-

- Dimensional J-Aggregate Monolayers of Cyanine Dyes. *Makrogeter-otsikly* **2012**, 5 (4–5), 371–376.
- (26) Wang, C.; Weiss, E. A. Accelerating FRET between Near-Infrared Emitting Quantum Dots Using a Molecular J-Aggregate as an Exciton Bridge. *Nano Lett.* **2017**, *17* (9), 5666–5671.
- (27) Kirstein, S.; Möhwald, H.; Shimomura, M. Crystalline Two-Dimensional Domains of Cyanine Dyes at Interfaces. *Chem. Phys. Lett.* **1989**, *154* (4), 303–308.
- (28) Kim, O. K.; Je, J.; Jernigan, G.; Buckley, L.; Whitten, D. Super-Helix Formation Induced by Cyanine J-Aggregates onto Random-Coil Carboxymethyl Amylose as Template. *J. Am. Chem. Soc.* **2006**, *128* (2), 510–516.
- (29) Garoff, R. A.; Litzinger, E. A.; Connor, R. E.; Fishman, I.; Armitage, B. A. Helical Aggregation of Cyanine Dyes on DNA Templates: Effect of Dye Structure on Formation of Homo- and Heteroaggregates. *Langmuir* **2002**, *18* (16), 6330–6337.
- (30) Hannah, K. C.; Armitage, B. A. DNA-Templated Assembly of Helical Cyanine Dye Aggregates: A Supramolecular Chain Polymerization. *Acc. Chem. Res.* **2004**, *37* (11), 845–853.
- (31) Didraga, C.; Pugžlys, A.; Hania, P. R.; von Berlepsch, H.; Duppen, K.; Knoester, J. Structure, Spectroscopy, and Microscopic Model of Tubular Carbocyanine Dye Aggregates. *J. Phys. Chem. B* **2004**, *108* (39), 14976–14985.
- (32) Eisele, D. M.; Cone, C. W.; Bloemsma, E. A.; Vlaming, S. M.; van der Kwaak, C. G. F.; Silbey, R. J.; Bawendi, M. G.; Knoester, J.; Rabe, J. P.; Vanden Bout, D. A. Utilizing Redox-Chemistry to Elucidate the Nature of Exciton Transitions in Supramolecular Dye Nanotubes. *Nat. Chem.* **2012**, *4* (8), 655–662.
- (33) Chuang, C.; Bennett, D. I. G.; Caram, J. R.; Aspuru-Guzik, A.; Bawendi, M. G.; Cao, J. Generalized Kasha's Model: T-Dependent Spectroscopy Reveals Short-Range Structures of 2D Excitonic Systems. *Chem.* **2019**, *5* (12), 3135–3150.
- (34) Eisele, D. M.; Knoester, J.; Kirstein, S.; Rabe, J. P.; Vanden Bout, D. A. Uniform Exciton Fluorescence from Individual Molecular Nanotubes Immobilized on Solid Substrates. *Nat. Nanotechnol.* **2009**, 4 (10), 658–663.
- (35) Chen, Z.; Lohr, A.; Saha-Möller, C. R.; Würthner, F. Self-Assembled  $\pi$ -Stacks of Functional Dyes in Solution: Structural and Thermodynamic Features. *Chem. Soc. Rev.* **2009**, 38 (2), 564–584.
- (36) Ben-Shaul, A.; Gelbart, W. M. Statistical Thermodynamics of Amphiphile Self-Assembly: Structure and Phase Transitions in Micellar Solutions. In *Micelles, Membranes, Microemulsions, and Monolayers*; Gelbart, W. M., Ben-Shaul, A., Roux, D., Eds.; Springer: New York, 1994; pp 1–104.
- (37) Israelachvili, J. N. Intermolecular and Surface Forces, 3rd ed.; Elsevier, 2011.
- (38) Montcuquet, A. S.; Hervé, L.; Navarro, F.; Dinten, J. M.; Mars, J. I. In Vivo Fluorescence Spectra Unmixing and Autofluorescence Removal by Sparse Nonnegative Matrix Factorization. *IEEE Trans. Biomed. Eng.* **2011**, 58 (9), 2554–2565.
- (39) Caram, J. R.; Doria, S.; Eisele, D. M.; Freyria, F. S.; Sinclair, T. S.; Rebentrost, P.; Lloyd, S.; Bawendi, M. G. Room-Temperature Micron-Scale Exciton Migration in a Stabilized Emissive Molecular Aggregate. *Nano Lett.* **2016**, *16* (11), 6808–6815.
- (40) Smulders, M. M. J.; Nieuwenhuizen, M. M. L.; De Greef, T. F. A.; Van Der Schoot, P.; Schenning, A. P. H. J.; Meijer, E. W. How to Distinguish Isodesmic from Cooperative Supramolecular Polymerisation. *Chem. Eur. J.* **2010**, *16* (1), 362–367.
- (41) Fukui, T.; Kawai, S.; Fujinuma, S.; Matsushita, Y.; Yasuda, T.; Sakurai, T.; Seki, S.; Takeuchi, M.; Sugiyasu, K. Control over Differentiation of a Metastable Supramolecular Assembly in One and Two Dimensions. *Nat. Chem.* **2017**, *9* (5), 493–499.